# The Impact of Rubidium and Cesium Cations on the Moisture Stability of Multiple-Cation Mixed-Halide Perovskites

*Yinghong Hu,[1] Meltem F. Aygüler,[1] Michiel L. Petrus,[1] Thomas Bein,[1] Pablo Docampo[2,*]*

[1] Department of Chemistry and Center for NanoScience (CeNS), LMU Munich, 81377 Munich, Germany.

[2] Physics Department, School of Electrical and Electronic Engineering, Newcastle University, Newcastle upon Tyne, NE1 7RU, United Kingdom.

**Corresponding Author**

* Pablo.Docampo@newcastle.ac.uk

Telephone: +44 (0) 191 20 88421

ABSTRACT

$Rb^+$ and $Cs^+$ have been recently identified as enhancers for perovskite solar cell performance. However, the impact of these inorganic cations on the stability of the $(FA_{0.83}MA_{0.17})Pb(I_{0.83}Br_{0.17})_3$ perovskite crystal lattice has not been fully understood yet. Here, we show via ~~that $Cs^+$ can stabilize the photoactive $(FA_{0.83}MA_{0.17})Pb(I_{0.83}Br_{0.17})_3$ phase through incorporation into the perovskite lattice, while the unsuitably small ionic radius of $Rb^+$ causes phase segregation~~. ~~*I*~~*in situ* XRD and EDX measurements ~~reveal~~ that the unsuitably small ionic radius of $Rb^+$ can lead to several non-photoactive side-products: $RbPb(I_{1-x}Br_x)_3$ during the perovskite formation and, a hitherto unreported $RbPb_2I_4Br$ phase which forms rapidly upon exposure to humid air. The Rb-rich side phases do not only result in absorbance loss, but also leach bromide ions away from the photoactive perovskite phase, thereby changing its bandgap. ~~While~~ In comparison, ~~Cs-addition~~ the moisture-assisted formation of a transparent $CsPb_2I_4Br$ phase upon Cs-addition occurs on a significantly longer timescale than the Rb-analog~~on~~ue. While the incorporation of cesium remains attractive for high-performance solar cells, the severe moisture ~~instability~~ sensitivity of mixed-cation perovskites upon Rb-addition may prove to be their Achilles' heel ~~already in the long~~short ~~term by hampering the fabrication process~~.

**TOC GRAPHICS**

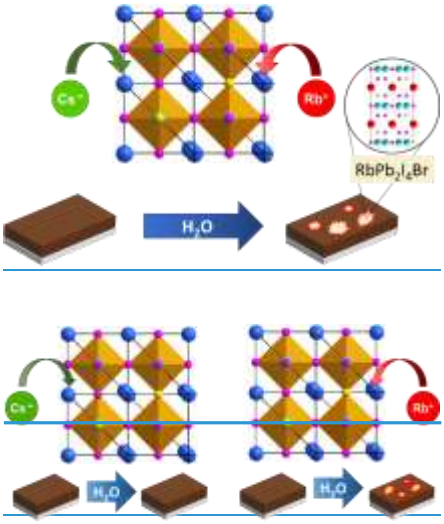
Cs+
Rb+
RbPb2I4Br
H2O
Cs+
Rb+
H2O
H2O

Recently, inorganic cations such as rubidium and cesium have been reported as performance enhancers in the burgeoning field of perovskite solar cells, both in terms of power conversion efficiency (PCE) and device stability.[1-9] An impressive improvement in open-circuit voltage ($V_{oc}$) was achieved through the addition of RbI and CsI to the multiple-cation mixed-halide $(FA_{0.83}MA_{0.17})Pb(I_{0.83}Br_{0.17})_3$ perovskite, reaching stabilized efficiencies up to 21.6%.[4,6] Mixing organic cations such as formamidinium or methylammonium with small amounts of $Rb^+$ or $Cs^+$ cations can lead to a more favorable tolerance factor which facilitates the stabilization of the photoactive perovskite phase in a broad temperature range,[3] resulting in devices stable at 85 °C for 500 hours under continuous illumination and maximum power tracking.[6] Yet, the complexity of the interplay between the different cations and halides increases significantly with every additional component that takes part in the perovskite formation. Therefore, the role of $Rb^+$ and $Cs^+$ cations within the perovskite's structure and their impact on the stability and optoelectronic properties are still under debate.

A simple, empirical measure for the stability of $ABX_3$ perovskite structures is Goldschmidt's tolerance factor[10]

$$t = \frac{r_A + r_X}{\sqrt{2}\,(r_B + r_X)}$$

with *r* being the ionic radius of each respective ion. Ionic compounds with a tolerance factor within the range between 0.8 and 1.0 are considered to be stable in a classical perovskite structure. For $CsPbI_3$ ($t = 0.81$), the tolerance factor suggests that $Cs^+$ can stabilize a classical perovskite structure consisting of corner-sharing lead-iodide octahedra.[3,11,12] Indeed, $CsPbI_3$ is known to undergo a phase transition from a room-temperature yellow phase into a black perovskite-type phase at 360 °C.[12-14] Upon Cs-insertion into $(FA_{0.83}MA_{0.17})Pb(I_{0.83}Br_{0.17})_3$, a contraction of the perovskite

crystal lattice can be expected due to the significantly smaller ionic radius of $Cs^+$ (167 pm) compared to $FA^+$ (~253 pm) and $MA^+$ (~217 pm) cations.[15] In contrast, $RbPbI_3$ achieves a lower tolerance factor of $t$ = 0.77 which indicates that $Rb^+$ (152 pm) is too small to stabilize this perovskite lattice, but instead leads to the formation of non-perovskite structures.[5,6] Furthermore, unlike its Cs-based counterpart, $RbPbI_3$ does not undergo a phase transition to a black perovskite structure at elevated temperatures.[2,16] Hence, the interaction of $Cs^+$ and $Rb^+$ with the iodide-dominated perovskite structure is potentially very different.

Understanding the effect of inorganic cations on the perovskite crystal lattice is not only crucial to boost solar cell performance, but also to eliminate potential degradation pathways. In this work, we elucidated the influence of $Rb^+$ and $Cs^+$ on the crystal structure of the state-of-the-art $(FA_{0.83}MA_{0.17})Pb(I_{0.83}Br_{0.17})_3$ hybrid perovskite compound. Furthermore, we investigated the impact of the inorganic cation additives on the perovskite's moisture stability and the resulting effects on solar cell performance. Our results show that in particular, the addition of rubidium cations to an iodide-bromide mixed-halide perovskite strongly affects the robustness of the perovskite phase toward humidity.

We synthesized the perovskite composition employed in state-of-the-art photovoltaic devices $(FA_{0.83}MA_{0.17})Pb(I_{0.83}Br_{0.17})_3$ (FAMA), and added a defined amount of RbI or/and CsI according to a protocol reported by Saliba *et al*.[6] We denote the samples as Rbx, Csx and CsxRbx, with x being the percentage of $Cs^+$ or $Rb^+$ among the monovalent cations.

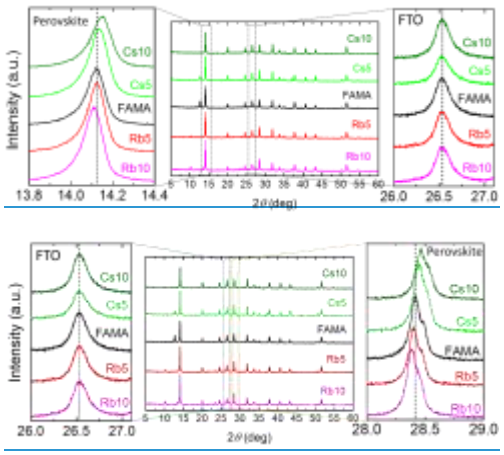


**Figure 1.** XRD patterns of multiple-cation mixed-halide perovskite films on glass/FTO/compact $TiO_2$ substrates upon addition of different amounts of RbI and CsI to the perovskite precursor solution. FAMA represents $(FA_{0.83}MA_{0.17})Pb(I_{0.83}Br_{0.17})_3$ and Csx (Rbx) refers to samples with the approximate molar percentage x of $Cs^+$ ($Rb^+$).

When it comes to the influence of the inorganic cations on the crystallization of the perovskite, one of the main questions that arises is: Are $Cs^+$ and $Rb^+$ cations incorporated into the perovskite structure? Modifications of the perovskite lattice dimensions upon addition of inorganic cations can be deduced from a shift in the X-ray diffraction (XRD) peaks of the perovskite phase.[3,6] To disclose this effect, we determined the exact XRD peak position of the ~~most intense~~(220~~0~~22) reflection for the FAMA perovskite film and compared it to samples with different amounts of added RbI and CsI (Figure 1). By using the (110) reflection of the FTO-glass substrate at $2\theta = 26.53°$ as a reference peak, we can exclude a misalignment of the experimental stage height as an

origin for any XRD peak shift. Upon Cs-addition to FAMA, we observe that the ~~main~~ reflection of the pristine FAMA perovskite phase at $2\theta$ = 28.41~~14.12~~° shifts to larger diffraction angles for Cs5 (28.45~~14.14~~°) and even further for Cs10 (28.47~~14.15~~°). This finding is in agreement with previous reports[3,4,17] and can be interpreted as an evidence for the inclusion of $Cs^+$ into the perovskite structure, therefore leading to a shrinkage of the perovskite lattice. The higher the $Cs^+$ concentration is in the perovskite precursor solution, the more pronounced is the shift to higher angles in the XRD pattern, and the larger is the contraction of the perovskite lattice. However, even more remarkable is ~~no significant~~the ~~-~~peak shift to lower angles ~~was~~ observed for Rb5 ($2\theta$ =28.40°) and~~.~~ ~~Even more remarkable is the shift to lower angles for~~ Rb10 ($2\theta$ = 28.38~~14.11~~°) ~~compared to FAMA~~, which indicates an expansion of the perovskite lattice compared to FAMA. The same trend is also visible in a shift of the main perovskite peak around 14.1° which is shown in Figure S1. Considering that $Rb^+$ has an even smaller ionic radius compared to $Cs^+$, we would expect an even stronger lattice contraction. Therefore, one could conclude that $Rb^+$ is not fully incorporated into the perovskite structure in contrast to $Cs^+$, although this does not explain the observed expansion of the crystal lattice.

In order to understand the shift to a lower angle of the perovskite lattice upon addition of $Rb^+$, we must look into the formation of the Rb-rich side phases. The XRD patterns of Rb5 and Rb10 exhibit an additional double peak at $2\theta$ = 10.16° and 10.29°, which is more prominent for Rb10. This is typically assigned to the yellow orthorhombic, non-perovskite $RbPbI_3$ phase.[1,2,16,18] However, we found that the characteristic (110) and (020) reflections of a freshly synthesized $RbPbI_3$ film are located at 10.03° and 10.20°, respectively (Figure ~~S1~~S2). Hence, the XRD reflections originating from the side phases in the Rb5 and Rb10 samples belong to a smaller lattice than the pure iodide compound $RbPbI_3$. Since the casting solution contains a mixture of $I^-$ and $Br^-$, it is reasonable to

propose that the Rb-rich side phase is a mixed-halide structure of the form $RbPb(I_{1-x}Br_x)_3$. An estimated Br-content of x ≈ 0.16 was found for the Rb-rich side phase in Rb10 and Rb5 by analyzing the XRD peak shift in spin-coated films from $RbPb(I_{1-x}Br_x)_3$ solutions with varying x (see Figure ~~S1~~S2). We note that this value corresponds to the approximate initial Br : I ratio in the perovskite precursor solution.

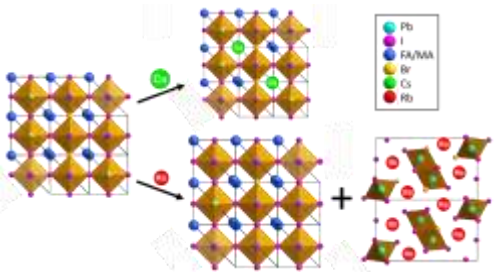


**Figure 2.** Schematic illustration of the effect of RbI and CsI addition on the multiple-cation mixed-halide perovskite structure. Lattice contraction by incorporation of $Cs^+$ cations into the perovskite structure vs. lattice expansion due to Br-extraction from the perovskite structure and formation of an Rb- and Br-rich non-perovskite side phase $RbPb(I_{1-x}Br_x)_3$.

Compared to $I^-$ ions (220 pm), the smaller $Br^-$ ions (196 pm) have a higher compatibility of ionic radius in combination with $Rb^+$, resulting in a slightly higher tolerance factor ($t$ = 0.78) and the existence of a high-temperature $RbPbBr_3$ perovskite phase.[19] This affinity between $Rb^+$ and $Br^-$ can have an enormous impact on the composition and the stability of multiple-cation mixed-halide perovskite compounds. When the Rb-concentration is as high as 10 mol% in Rb10, the formation

of the $RbPb(I_{0.84}Br_{0.16})_3$ phase has leached a sufficiently large amount of bromide away from the perovskite lattice, such that an effective expansion of the (now I-rich) perovskite structure occurs, explaining the left shift of its XRD main peak. Figure 2 represents a schematic illustration of the effect of CsI and RbI addition on the lattice dimensions of the FAMA perovskite phase. Our hypothesis is perfectly consistent with previous observations by Duong *et al.*[5] The latter authors also report a systematic red shift of both the photoluminescence peak and the absorption onset of the mixed-halide perovskite upon increased Rb-concentration, which can be related to a reduction of the Br-content within the perovskite through $RbPb(I_{0.84}Br_{0.16})_3$ formation. In contrast, due to the more suitable size of the $Cs^+$ ion to be incorporated into the perovskite lattice, neither Cs5 nor Cs10 exhibit a comparable side phase resulting from phase separation.

The instability of the perovskite lattice upon Rb-inclusion is further highlighted by exposing the perovskite films to humid air. Here, we performed *in situ* XRD measurements on FAMA, Cs5, Rb5 and Rb5Cs5 films upon exposure to air at 75% relative humidity (RH) to determine the degradation products. In order to exclude the influence of ambient light on the degradation process,[20] the humidity studies were conducted in the dark. Figure 3 depicts the evolution of the XRD patterns for each sample prepared on glass substrates over a period of 60 min. Both FAMA and Cs5 show minor signs of degradation after 60 min, visible in a slightly increased $PbI_2$ peak at $2\theta = 12.7°$. In contrast, a strong reflection at 11.4° emerges for the Rb5 and the Rb5Cs5 film after only 15 min, and additional reflections at 22.9°, 34.7° and 46.8° appear upon longer exposure times.

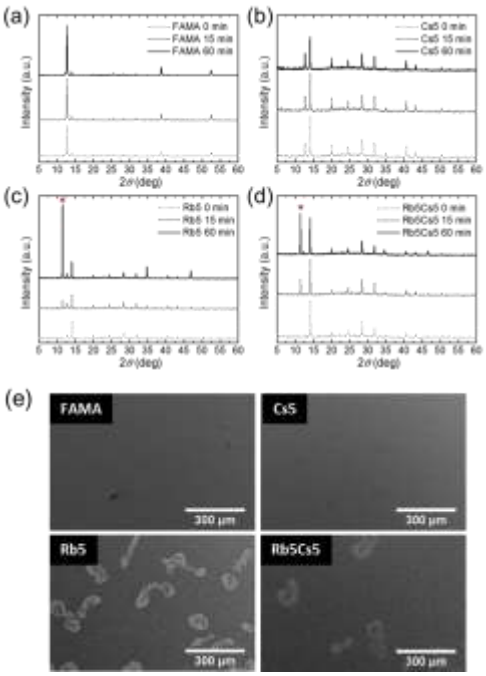


**Figure 3.** XRD patterns of (a) FAMA, (b) Cs5, (c) Rb5 and (d) Rb5Cs5 perovskite films on glass under *in situ* exposure to air at 75% RH over a course of 60 min. The most intense diffraction peak assigned to the moisture-induced degradation product for the Rb-containing samples is marked with a red asterisk ~~(*)~~. (e) SEM top-view images of perovskite films on glass/FTO/$TiO_2$ after exposure to humid air with 90% RH for 20 h.

These additional diffraction peaks can also be found at lower or higher humidity levels (Figure ~~S2~~S3) and are accompanied by the formation of transparent spots on the dark brown perovskite films that can be seen with the bare eye. Top-view SEM images of Rb5 and Rb5Cs5 films on FTO/$TiO_2$ substrates reveal the presence of irregularly shaped, bright areas (~100 µm in diameter)

after exposing the samples to 90% RH for 20 h (Figure 3e). For comparison, FAMA and Cs5 do not show such inhomogeneity under the same conditions. Only after longer exposure times of 5 days, the Cs5 film exhibited some transparent imperfections and the corresponding XRD pattern showed a set of additional reflections at $2\theta$ = 11.2°, 33.9° and 45.7° (Figure ~~S3~~S4), similar to the degradation product found on the Rb-containing samples.

To understand the mechanism that induces the phase segregation within the perovskite films upon exposure to moisture, it is crucial to determine the chemical composition of the degradation products. Energy dispersive X-ray (EDX) spectroscopy is a powerful tool to assess the chemical composition of thin films with a µm-range spatial resolution. We determined the elemental composition of intact areas and, if present, phase separated ("degraded") areas for each perovskite sample by EDX measurements (Table S1) to identify the moisture-induced degradation products. Details on the EDX analysis, SEM images of the evaluated sample areas and EDX spectra are provided in the Supporting Information (Figures ~~S4~~S5-~~5~~6).

Table 1 shows that all samples exhibit a comparable Pb : I : Br ratio in their intact areas, corresponding to the precursor stoichiometry used in the perovskite solution. After exposure to 90% RH for 2 days, FAMA does not change its elemental stoichiometry and no apparent phase separation is observed. However, we found significant differences between the elemental composition of the intact and the degraded areas of Rb5 and Rb5Cs5 after the moisture-induced phase segregation after 20 h. Compared to the intact areas, the degraded areas of Rb-containing samples show to be Rb- and Br-rich. More specifically, the Rb-content is increased from ~0% to 12–14% and the I-content is decreased from ~60% to ~50% in the degraded areas of Rb5 and Rb5Cs5, while the Br-content was constant (~13%). After a significant longer exposure time of 5 days, the degraded areas in the Cs5 sample showed a Cs- and Br-rich phase separation product

with a comparable chemical composition as the one found in the Rb-containing perovskites. We note that, similar to $RbPb(I_{1-x}Br_x)_3$, the moisture-mediated formation of the Br-rich phase with either CsI or RbI replaces a significant amount of bromide the perovskite lattice with iodide, leading to a noticeable shift of the XRD peak to lower angles (Figure ~~S6~~S7). Another indication for the loss of bromide within the perovskite structure after hydration of Rb5 and Rb5Cs5 is a decreased bandgap of the perovskite phase, as revealed by the corresponding Tauc plots (Figure ~~S7~~S8).

Using the atomic composition determined for the degraded areas in Rb5, Rb5Cs5 and Cs5 from our EDX measurements (Table S1), we propose the chemical formula "$RbPb_2I_4Br$" and "$CsPb_2I_4Br$" for the phase segregation products. We suggest that these hitherto unreported crystal phases can be derived from the known compounds $RbPb_2Br_5$ and $CsPb_2Br_5$ by partially substituting bromide for iodide. The tetragonal crystal phase of $RbPb_2Br_5$ and $CsPb_2Br_5$ were first synthesized and characterized by Wells, obtained from the reaction of RbBr or CsBr with 2 equivalents of $PbBr_2$.[21-23] The reported transparency and water-stability of $RbPb_2Br_5$ and $CsPb_2Br_5$ crystals are in accordance with the properties we found for the moisture-induced phase separation products in Rb5, Rb5Cs5 and Cs5.

In order to verify the proposed formula $RbPb_2I_4Br$ (and $CsPb_2I_4Br$) derived from our EDX data, we spin-coated films derived from precursor solutions with the corresponding stoichiometry of RbI (CsI) : $PbI_2$ : $PbBr_2$ = 1 : 1.5 : 0.5. Strikingly, the XRD patterns of the resulting films exhibit exactly the same reflection at $2\theta = 11.45°$ (11.20°) that is found for hydrated Rb5 (Cs5) samples, as shown in Figure ~~S8~~S9. Thus, our proposed chemical formula for $RbPb_2I_4Br$ and $CsPb_2I_4Br$ are confirmed. As shown in previous moisture-stability studies, the presence of water molecules can significantly facilitate a reorganization and recrystallization of the perovskite grains.[24] Therefore,

moisture can promote rapid phase separation within the perovskite film under the formation of thermodynamically more favorable products. The spontaneous crystallization of $RbPb_2I_4Br$ simply from a stoichiometric precursor solution even without the aid of water indicates a strong driving force towards the formation of this compound. A schematic illustration of our proposed degradation route for Rb-containing FAMA perovskite films is depicted in Figure 4.

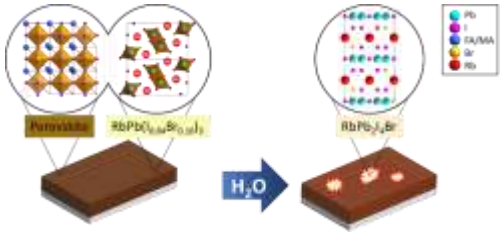


**Figure 4.** Schematic illustration of the moisture-induced degradation of Rb-containing multi-cation mixed-halide perovskite films.

It is important to note that the segregation of the $CsPb_2I_4Br$ phase takes place during a significantly longer timescale than $RbPb_2I_4Br$. Moreover, the $CsPb_2I_4Br$ phase was not observed in Rb5Cs5 samples after 20 h at 90% RH despite of the Rb : Cs ratio of 1 : 1, indicating that it is $Rb^+$ that induces rapid phase segregation first when water can act as a mediator. In the absence of bromide, degradation only took place with the emergence of $RbPbI_3$, $PbI_2$ and the yellow δ-phase of formamidinium lead iodide (Figure ~~S9~~S10).[25] This observation provides further evidence for the strong affinity of $Rb^+$ to $Br^-$ as discussed above regarding the $RbPb(I_{1-x}Br_x)_3$ formation.

To investigate the effect of moisture-induced $RbPb_2I_4Br$ formation on the photovoltaic performance of perovskite solar cells, we fabricated devices with the architecture

glass/FTO/$TiO_2$/perovskite/spiro-OMeTAD/Au. A full experimental description of the device fabrication and current-voltage (*J-V*) characterization are given in the Supporting Information. The as-prepared solar cells all show high performance with power conversion efficiency (PCE) values up to 17.75%. The corresponding *J-V* curves and the stabilized power output are displayed in the Supporting Information (Figures S10–11). We stored the unencapsulated devices (~~12~~ 24 cells for each type of perovskite) in a humidity chamber with controlled 75% RH at room temperature and monitored the average PCE and short-circuit current density ($J_{sc}$) of the solar cells over ~~3~~ 10 days. Figure 5a shows the appearance of transparent spots in the Rb5 and Rb5Cs5 samples after only ~~1~~ one day, indicating advanced segregation of $RbPb_2I_4Br$ (as evidenced by XRD, see Figure ~~S12~~S13). The partial transformation of the black perovskite phase into the ~~photo-inactive~~ $RbPb_2I_4Br$ phase leads to an irreversible ~~-~~loss of ~~light-absorbance~~photoactive material. This is accompanied by a notable decrease in PCE already after one day exposure to 75% RH for the Rb5 and Rb5Cs5 devices that can be linked to a loss of $J_{sc}$ (Figures 5b–c). After ~~3~~ 10 days, the Rb5 and Rb5Cs5 devices exhibit only ~~68~~18% and ~~52~~6% of their original average PCE values, respectively, compared to ~~88~~45% for FAMA and ~~74~~37% for Cs5. The further decreased performance of Rb5Cs5 compared to the Rb-only devices could be explained by the presence of $Cs^+$ in Rb5Cs5 films which enables additional degradation pathways through the formation of $CsPb_2I_4Br$. For the same reason, the Cs5 devices show a slightly larger decrease in photovoltaic performance than FAMA after more than 4 days at 75% RH. We observed the severe initial drop in PCE for Rb-containing solar cells also after one day at 58% RH (Figure S14), indicating that device degradation through $RbPb_2I_4Br$ formation already takes place at a lower humidity level. Our results demonstrate that moisture-induced phase separation within the perovskite material can strongly affect the photovoltaic performance of perovskite solar cells, even before chemical decomposition of the

perovskite (*e.g.* loss of the organic cations FA and MA) commences. We note that water plays a critical role as a mediator in the phase separation process, since all devices stored under nitrogen at room temperature retain 95% of their initial performance even after 5 months (Figure S15). Previous stability tests on Cs- and Rb-containing perovskite solar cells reported by Saliba *et al.* were conducted under the exclusion of water in a dry nitrogen atmosphere. Considering the different testing conditions, the previously observed improvement in ~~e.g. thermal~~device stability does not contradict our findings on the ~~moisture~~ stability of multi-cation mixed halide perovskites under exposure to moisture.

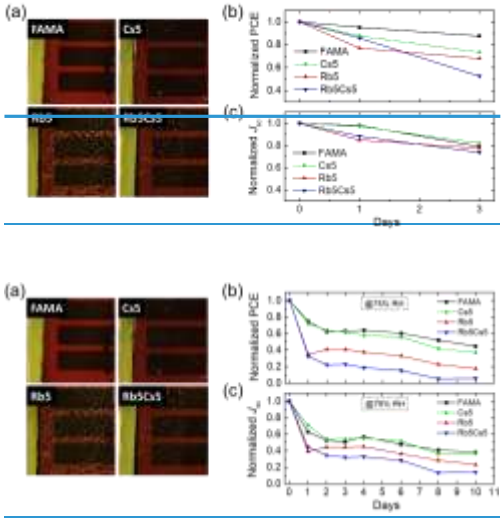


**Figure 5.** Moisture stability test on unencapsulated perovskite solar cells at 75% RH in air at room temperature in the dark. (a) Photographs of the devices after ~~1~~ one day. (b) Evolution of the normalized power conversion efficiency and (c) short-circuit current density upon humidity

**Formatted:** Normal, Space After: 0 pt

exposure for ~~3~~ 10 days. The efficiency values were obtained from *J-V* scans in the reverse direction with a scanning rate of 0.2 V $s^{-1}$.

Formatted: Font: Italic

In conclusion, the present study suggests that $Cs^+$ cations are incorporated into the multiple-cation mixed-halide $(FA_{0.83}MA_{0.17})Pb(I_{0.83}Br_{0.17})_3$ perovskite structure, leading to lattice contraction and stabilization of the photoactive perovskite phase. In contrast, RbI-addition induces the formation of non-photoactive, non-perovskite side phases such as $RbPb(I_{0.84}Br_{0.16})_3$ during film crystallization and $RbPb_2I_4Br$ upon moisture exposure. The origin of the facile phase separation could be the affinity between Rb and Br due to their more compatible ionic radii, which leads to thermodynamically more stable compounds than an iodide-based perovskite structure incorporating Rb. We demonstrate that the instability of Rb-containing mixed-halide perovskites opens up new degradation pathways through rapid phase segregation which can affect device performance long before notable chemical decomposition of the perovskite takes place. The severe moisture sensitivity of Rb-incorporating perovskites cannot be counteracted through simple device encapsulation, but requires strictly controlled humidity levels during and after perovskite film processing. This bedevils the fabrication process for low-cost perovskite solar cells.

Furthermore, our results indicate that Rb can cause a Br-deficiency in the mixed-halide perovskite structure via formation of the Br-rich side phases. Viewed from a more general perspective, our results can have significant implications for photovoltaic applications using mixed-halide perovskite such as in tandem solar cells, where the desired bandgap of the perovskite material is tailored by a defined halide ratio.[9] Therefore, we need to consider the choice of cations while taking into account the interplay between the different components for the perovskite formation.

Directing the focus on both short-term and long-term device stability will be important for moving perovskite-based photovoltaics closer toward commercial applications.

## EXPERIMENTAL METHODS

### Perovskite precursor solutions

The organic cation salts formamidinium iodide (FAI) and methylammonium bromide (MABr) were purchased from Dyesol, the lead halide compounds from TCI, CsI (99.9%) from Sigma-Aldrich and RbI from abcr GmbH. All chemicals were used without further purification.

**FAMA:** Following the protocol reported by Saliba *et al.*,[6] a multiple cation mixed-halide perovskite solution was prepared. $PbI_2$ (508 mg, 1.1 mmol), $PbBr_2$ (80.7 mg, 0.22 mmol), FAI (171.97 mg, 1 mmol) and MABr (22.4 mg, 0.2mmol) were dissolved in 800 µL of anhydrous DMF and 200 µL DMSO by heating the solution up to 100 °C. This nonstoichiometric $(FA_{0.83}MA_{0.17})Pb(I_{0.83}Br_{0.17})_3$ precursor solution contains a 10 mol% excess of $PbI_2$ and $PbBr_2$, respectively, which was introduced to enhance device performance. The FAMA solution was filtrated through a 0.45 µm syringe filter before usage.

**Cs5 and Cs10:** CsI (389.7 mg, 1.5 mmol) was dissolved in 1 mL DMSO and filtrated through a 0.45 µm syringe filter, yielding an approximately 1.5 M CsI stock solution. To obtain the desired triple cation perovskite composition of approximately 5 mol% Cs, 42 µL of the CsI stock solution was added to 1 mL FAMA solution, yielding a nominal composition of $Cs_{0.05}[(FA_{0.83}MA_{0.17})]_{0.95}Pb(I_{0.83}Br_{0.17})_3$ for Cs5. The precursor solution for Cs10 was obtained by adding 84 µL of the CsI solution to 1 mL FAMA solution.

**Rb5 and Rb10:** RbI (318.5 mg, 1.5 mmol) was dissolved in 1 mL of a 4 : 1 (v/v) DMF : DMSO mixture and filtrated through a 0.45 µm syringe filter. To obtain the desired triple cation perovskite composition of 5% Rb, 42 µL of the 1.5 M RbI stock solution was added to 1 mL FAMA solution, yielding a nominal composition of $Rb_{0.05}[(FA_{0.83}MA_{0.17})]_{0.95}Pb(I_{0.83}Br_{0.17})_3$ for Rb5. The precursor solution for Rb10 was obtained by adding 84 µL of the RbI solution to 1 mL FAMA solution.

**Rb5Cs5:** To obtain the quadruple cation perovskite composition of 5% Rb and 5% Cs, 42 µL of the RbI stock solution and 42 µL of the CsI stock solution were added to 1 mL FAMA solution, yielding a nominal composition of $Rb_{0.05}Cs_{0.05}[(FA_{0.83}MA_{0.17})]_{0.9}Pb(I_{0.83}Br_{0.17})_3$.

### Film Fabrication

The deposition of the perovskite layer was processed in a nitrogen-filled glovebox at a controlled temperature of 20–23 °C. The perovskite solution was deposited in a consecutive two-step spin-coating process at 1000 rpm and 4000 rpm for 10 s and 30 s, respectively. Approximately 20 s

before the end of spinning, 500 µL of chlorobenzene (anhydrous, Sigma-Aldrich, 99.8%) was added to the film. The perovskite film formation was completed after annealing at 100 °C for 60 min on a hotplate.

To fabricate $RbPb(I_{1-x}Br_x)_3$ films, 1 M $RbPb(I_{1-x}Br_x)_3$ solutions with different Br-contents were prepared by dissolving RbI, $PbBr_2$ and $PbI_2$ in a DMF : DMSO 4:1 (v/v) mixture with the corresponding stoichiometry. For 1 mL solution, the amount of RbI (212.4 mg, 1 mmol) was held constant, while the $PbBr_2$ : $PbI_2$ ratio was varied to obtain final Br-contents of x = 0.16 (88.1 mg : 350.4 mg), x = 0.20 (110.1 mg : 322.7 mg) and x = 0.25 (137.6 mg : 288.1 mg), respectively. After dissolving the components at 100 °C, the same spin-coating procedure as for the perovskite films was conducted and the films were annealed at 100 °C for 60 min. Pale yellow films were obtained.

To reproduce the crystal phases $RbPb_2I_4Br$ found as products of moisture-induced phase separation in Rb5 and Rb5Cs5 samples, a stoichiometric solution of RbI : $PbI_2$ : $PbBr_2$ = 1 : 1.5 : 0.5 was prepared. Therefore, RbI (106.18 mg, 0.5 mmol), $PbI_2$ (345.7 mg, 0.75 mmol) and $PbBr_2$ (91.75 mg, 0.25 mmol) were dissolved in 0.5 mL of a 4 :1 (v/v) DMF : DMSO mixture. Then the same spin-coating procedure as for the perovskite films was conducted (without the chlorobenzene drip) and the samples were annealed at 100 °C for 10 min, yielding pale yellow films. For the reproduction of the $CsPb_2I_4Br$ phase, RbI was replaced by CsI (129.9 mg, 0.5 mmol).

Device Fabrication

Fluorine-doped tin oxide (FTO) coated glass substrates (7 Ω/sq) were patterned by etching with zinc powder and 3 M HCl solution and successively cleaned with deionized water, a 2% Hellmanex detergent solution, ethanol and finally treated with oxygen plasma for 5 min. A compact $TiO_2$ layer was deposited as hole blocking layer on the substrate *via* a sol-gel approach. Therefore, a mixture of 2 M HCl (35 µL) and anhydrous isopropanol (2.53 mL) was added dropwise to a solution of 370 µL titanium(IV) isopropoxide (Sigma-Aldrich) in isopropanol (2.53 mL) under vigorous stirring. The filtrated $TiO_x$ solution was spin-coated dynamically onto the FTO substrates at 2000 rpm for 45 s, followed by annealing in air at 150 °C for 10 min and subsequently at 500 °C for 45 min.

The deposition of the perovskite layer was conducted as described above for the thin film fabrication.

For the hole transporter layer, 1 mL solution of 2,2',7,7'-tetrakis-(*N,N*-di-*p*-methoxyphenyl-amine)-9,9'-spirobifluorene (spiro-OMeTAD, Borun Chemicals, 99.8%) in anhydrous chlorobenzene (75 mg/mL) was doped with 10 µL 4-*tert*-butylpyridine (Sigma-Aldrich, 96%) and 30 µL of a 170 mg/mL lithium bistrifluoromethanesulfonimidate (Li-TFSI) (Sigma-Aldrich, 99.95%) solution in acetonitrile (Sigma-Aldrich, anhydrous) and deposited by spin-coating at 1500 rpm for 40 s and then 2000 rpm for 5 s. After storing the samples overnight in air at 25% relative humidity, 40 nm Au was deposited through a patterned shadow mask by thermal evaporation at $8 \cdot 10^{-7}$ mbar to form the back electrode.

Film Characterization

X-ray diffraction (XRD) measurements of thin films were performed with a Bruker D8 Discover X-ray diffractometer operating at 40 kV and 30 mA, employing Ni-filtered Cu K $_{\alpha 1}$ radiation ($\lambda$ = 1.5406 Å) and a position-sensitive LynxEye detector. A step size of $\Delta 2\theta$ = 0.0026° was employed to resolve the change in peak position of the perovskite's diffraction peak. For the *in situ* XRD measurements during the hydration process, a custom-made hydration chamber made of X-ray transparent polymers with a total volume around 250 mL was utilized. The air humidity within the hydration chamber was held constant employing vials filled with saturated salt solutions and measured using a hygrometer. The salts $Na_2CO_3$, NaCl, NaBr and $K_2CO_3$ were used for controlling the humidity level to 92%, 75%, 58% and 45% RH, respectively. All experiments were performed at room temperature (21 °C) without illumination.

Scanning electron microscopy (SEM) images were recorded with an FEI Helios Nanolab G3 UC DualBeam scanning electron microscope, operated at an acceleration voltage of 5 keV. EDX spectra were recorded and evaluated with an Oxford Instruments AZTEC EDX-system. For EDX investigations, the samples were tilted to an angle of 52° with respect to the electron beam and an acceleration voltage of 20 keV was employed.

Ultraviolet-visible (UV-Vis) absorption spectra were recorded using a Perkin Elmer Lambda 1050 spectrophotometer equipped with a 150 mm integrating sphere. The perovskite samples for UV-Vis spectra measurements were fabricated on cleaned microscope glass slides.

Device Characterization

Current-Voltage (*J-V*) curves were recorded under ambient conditions using a Newport OrielSol 2A solar simulator with a Keithley 2400 source meter under simulated AM 1.5G sunlight, with an incident power of 100 mW cm$^{-2}$, calibrated with a Fraunhofer ISE certified silicon cell (KG5-filtered). The active area of the solar cells was defined with a square metal aperture mask of 0.0831 cm$^2$. After pre-biasing the device at 1.3 V for 5 s under illumination, *J-V* curves were recorded by scanning the input bias from 1.3 V to 0 V (reverse scan) and then from 0 V to 1.3 V (forward scan) at a scan rate of 0.1 V s$^{-1}$. All as-prepared devices show a comparable degree of hysteresis between the forward and reverse scan (Figure S10). The stabilized power output was measured by tracking the current at the maximum power point (Figure S11) under 1 sun illumination without pre-biasing the device.

Humidity studies on the perovskite solar cells were conducted in a ~~shaded~~ glass container at a constant humidity level of 75% RH in air that was maintained by a saturated aqueous NaCl solution at the bottom of the jar. Humidity stability tests at 58% RH were performed in the same way using a NaBr solution. In order to exclude the influence of light exposure on the degradation process, the container was kept in the dark. The unencapsulated solar cells were placed onto a stage inside the sealed container being exposed to the moist air and without having direct contact with the solution. After a certain exposure time, the *J-V* curves of the devices were measured under ambient conditions and 1 sun illumination ~~as described above~~at a scan rate of 0.2 V s$^{-1}$. ~~12~~ 24 ~~pixels~~ cells were evaluated for each type of perovskite solar cell for 75% RH and 20 cells for 58% RH. ~~and t~~The arithmetic means of the PCE and $J_{sc}$ values extracted from the reverse *J-V* scans were ~~compared~~monitored over a course of 10 days. The stability of devices under the exclusion of water

Formatted: Superscript

Formatted: Font: Italic

was determined by measuring the PCE of 20 cells for each type of perovskites after storage in a nitrogen-filled glovebox for 5 months.

## ASSOCIATED CONTENT

**Supporting Information**. Additional XRD patterns, SEM images, EDX data, Tauc plots, *J-V* curves, stabilized power output of solar cells. The Supporting Information is available free of charge via the internet at http://pubs.acs.org.

## AUTHOR INFORMATION

Corresponding author

*E-mail: Pablo.Docampo@newcastle.ac.uk

Website: https://blogs.ncl.ac.uk/pablodocampo/

### Notes

The authors declare no competing financial interests.

## ACKNOWLEDGMENT

The authors specially thank Dr. Steffen Schmidt from the LMU Munich for SEM and EDX measurements. This project was financed by a grant from the German Federal Ministry of Education and Research (BMBF) under the project ID 03SF0516B. The authors acknowledge funding from the Bavarian Collaborative Research Program "Solar Technologies Go Hybrid" (SolTech), the Center for NanoScience (CeNS), and the DFG Excellence Cluster "Nanosystems Initiative Munich" (NIM). M.F.A. acknowledges the Scientific and Technological Research Council of Turkey. P. D. acknowledges support from the European Union through the award of a Marie Curie Intra-European Fellowship.

REFERENCES

(1) Zhang, M.; Yun, J. S.; Ma, Q.; Zheng, J.; Lau, C. F. J.; Deng, X.; Kim, J.; Kim, D.; Seidel, J.; Green, M. A.; Huang, S. and Ho-Baillie, A. W. Y. High-Efficiency Rubidium-Incorporated Perovskite Solar Cells by Gas Quenching. *ACS Energy Lett.* **2017**, 438-444.

(2) Park, Y. H.; Jeong, I.; Bae, S.; Son, H. J.; Lee, P.; Lee, J.; Lee, C.-H. and Ko, M. J. Inorganic Rubidium Cation as an Enhancer for Photovoltaic Performance and Moisture Stability of HC(NH2)2PbI3 Perovskite Solar Cells. *Adv. Funct. Mater.* **2017**, 1605988.

(3) Li, Z.; Yang, M.; Park, J.-S.; Wei, S.-H.; Berry, J. J. and Zhu, K. Stabilizing Perovskite Structures by Tuning Tolerance Factor: Formation of Formamidinium and Cesium Lead Iodide Solid-State Alloys. *Chem. Mater.* **2016**, *28*, 284-292.

(4) Saliba, M.; Matsui, T.; Seo, J.-Y.; Domanski, K.; Correa-Baena, J.-P.; Nazeeruddin, M. K.; Zakeeruddin, S. M.; Tress, W.; Abate, A.; Hagfeldt, A. and Gratzel, M. Cesium-containing triple cation perovskite solar cells: improved stability, reproducibility and high efficiency. *Energy. Environ. Sci.* **2016**, *9*, 1989-1997.

(5) Duong, T.; Mulmudi, H. K.; Shen, H.; Wu, Y.; Barugkin, C.; Mayon, Y. O.; Nguyen, H. T.; Macdonald, D.; Peng, J.; Lockrey, M.; Li, W.; Cheng, Y.-B.; White, T. P.; Weber, K. and Catchpole, K. Structural engineering using rubidium iodide as a dopant under excess lead iodide conditions for high efficiency and stable perovskites. *Nano Energy* **2016**, *30*, 330-340.

(6) Saliba, M.; Matsui, T.; Domanski, K.; Seo, J.-Y.; Ummadisingu, A.; Zakeeruddin, S. M.; Correa-Baena, J.-P.; Tress, W. R.; Abate, A.; Hagfeldt, A. and Grätzel, M. Incorporation of rubidium cations into perovskite solar cells improves photovoltaic performance. *Science* **2016**, *354*, 206-209.

(7) Lee, J.-W.; Kim, D.-H.; Kim, H.-S.; Seo, S.-W.; Cho, S. M. and Park, N.-G. Formamidinium and Cesium Hybridization for Photo- and Moisture-Stable Perovskite Solar Cell. *Adv. Energy Mater.* **2015**, *5*, 1501310.

(8) Yi, C.; Luo, J.; Meloni, S.; Boziki, A.; Ashari-Astani, N.; Gratzel, C.; Zakeeruddin, S. M.; Rothlisberger, U. and Gratzel, M. Entropic stabilization of mixed A-cation ABX3 metal halide perovskites for high performance perovskite solar cells. *Energy. Environ. Sci.* **2016**, *9*, 656-662.

(9) McMeekin, D. P.; Sadoughi, G.; Rehman, W.; Eperon, G. E.; Saliba, M.; Hörantner, M. T.; Haghighirad, A.; Sakai, N.; Korte, L.; Rech, B.; Johnston, M. B.; Herz, L. M. and Snaith, H. J. A mixed-cation lead mixed-halide perovskite absorber for tandem solar cells. *Science* **2016**, *351*, 151-155.

(10) Goldschmidt, V. M. Die Gesetze der Krystallochemie. *Naturwissenschaften* **1926**, *14*, 477-485.

(11) Kieslich, G.; Sun, S. and Cheetham, A. K. Solid-state principles applied to organic-inorganic perovskites: new tricks for an old dog. *Chem. Sci.* **2014**, *5*, 4712-4715.

(12) Trots, D. M. and Myagkota, S. V. High-temperature structural evolution of caesium and rubidium triiodoplumbates. *J. Phys. Chem. Solids* **2008**, *69*, 2520-2526.

(13) Eperon, G. E.; Paterno, G. M.; Sutton, R. J.; Zampetti, A.; Haghighirad, A. A.; Cacialli, F. and Snaith, H. J. Inorganic caesium lead iodide perovskite solar cells. *J. Mater. Chem. A* **2015**, *3*, 19688-19695.

(14) Swarnkar, A.; Marshall, A. R.; Sanehira, E. M.; Chernomordik, B. D.; Moore, D. T.; Christians, J. A.; Chakrabarti, T. and Luther, J. M. Quantum dot–induced phase stabilization of α-CsPbI<sub>3</sub> perovskite for high-efficiency photovoltaics. *Science* **2016**, *354*, 92-95.

(15) Kieslich, G.; Sun, S. and Cheetham, A. K. An extended Tolerance Factor approach for organic-inorganic perovskites. *Chem. Sci.* **2015**, *6*, 3430-3433.

(16) Haupt, H. J.; Huber, F. and Preut, H. Darstellung und Kristallstruktur von Rubidiumtrijodoplumbat(II). *Z. Anorg. Allg. Chem.* **1974**, *408*, 209-213.

(17) Chang, Y.; Wang, L.; Zhang, J.; Zhou, Z.; Li, C.; Chen, B.; Etgar, L.; Cui, G. and Pang, S. CH3NH2 Gas Induced (110) Preferred Cesium-Containing Perovskite Film with Reduced PbI6 Octahedron Distortion and Enhanced Moisture Stability. *J. Mater. Chem. A* **2017**, *5*, 4803-4808.

(18) Brgoch, J.; Lehner, A. J.; Chabinyc, M. and Seshadri, R. Ab Initio Calculations of Band Gaps and Absolute Band Positions of Polymorphs of RbPbI3 and CsPbI3: Implications for Main-Group Halide Perovskite Photovoltaics. *J. Phys. Chem. C* **2014**, *118*, 27721-27727.

(19) Cola, M.; Massarotti, V.; Riccardi, R. and Sinistri, C. Binary Systems Formed by Lead Bromide with (Li, Na, K, Rb, Cs and Tl)Br: a DTA and Diffractometric Study. *Z. Naturforsch. A* **1971**, *26*, 1328.

(20) Wang, S.; Jiang, Y.; Juarez-Perez, Emilio J.; Ono, Luis K. and Qi, Y. Accelerated degradation of methylammonium lead iodide perovskites induced by exposure to iodine vapour. **2016**, *2*, 16195.

(21) Wells, H. L. On the caesium- and the potassium-lead halides. *Am. J. Sci.* **1893**, *45*, 121-134.

(22) Powell, H. M. and Tasker, H. S. 25. The valency angle of bivalent lead: the crystal structure of ammonium, rubidium, and potassium pentabromodiplumbites. *J. Chem. Soc.* **1937**, 119-123.

(23) Wells, H. L. On the rubidium-lead halides, and a summary of the double halides of lead. *Am. J. Sci.* **1893**, *Series 3 Vol. 46*, 34-38.

(24) Petrus, M. L.; Hu, Y.; Moia, D.; Calado, P.; Leguy, A. M. A.; Barnes, P. R. F. and Docampo, P. The Influence of Water Vapor on the Stability and Processing of Hybrid Perovskite Solar Cells Made from Non-Stoichiometric Precursor Mixtures. *ChemSusChem* **2016**, *9*, 2699-2707.

(25) Binek, A.; Hanusch, F. C.; Docampo, P. and Bein, T. Stabilization of the Trigonal High-Temperature Phase of Formamidinium Lead Iodide. *J. Phys. Chem. Lett.* **2015**, *6*, 1249-1253.